

Discriminating same-mass neutron stars and black holes gravitational waveforms

J.-F. Coupechoux^{1,*}, A. Arbey^{1,2,3}, R. Chierici¹, H. Hansen¹, J. Margueron¹, and V. Sordini¹

¹Univ Lyon, Univ Claude Bernard Lyon 1, CNRS/IN2P3, Institut de Physique des 2 Infinis de Lyon, UMR 5822, 69622 Villeurbanne, France

²Theoretical Physics Department, CERN, CH-1211 Geneva 23, Switzerland

³Institut Universitaire de France, 103 boulevard Saint-Michel, 75005 Paris, France

 (Received 19 July 2021; revised 26 January 2022; accepted 1 March 2022; published 30 March 2022)

Gravitational waveforms from coalescences of binary black hole and binary neutron star systems with low tidal effects can hardly be distinguished if the two systems have similar masses. In the absence of discriminating power based on the gravitational waveforms, the classification of sources into binary neutron stars, binary black holes and mixed systems can only be unambiguous when assuming the standard model of stellar evolution and using the fact that there exists a mass gap between neutron stars and black holes. This approach is however limited by its own assumptions: for instance the 2.6 solar mass object detected in the GW190814 event remains unclassified, and models of new physics can introduce new compact objects, like primordial black holes, which may have masses in the same range as neutron stars. In what follows, we investigate the possibility of discriminating between gravitational-wave signals emitted by different systems. First, we study the match between two waveforms, assuming several sensitivities of the detectors. In a second step, the ability of distinguishing one signal from the other is evaluated on simulations: a gravitational-wave signal is added to realistic noise from the LIGO-Virgo detectors, and the model best describing the simulated data is chosen based on the Bayes factor. The results depend strongly on the considered parameters, as the masses of the objects and tidal deformabilities of the neutrons stars. The task of distinguishing the nature of a compact object based on the gravitational-wave signal appears challenging for the current interferometers network. For instance, for a BNS system with tidal deformabilities $\Lambda = 600$ and chirp mass $1.44 M_{\odot}$ and under optimistic assumptions, the nature of compact objects is correctly determined only for distances smaller than 150 Mpc, while it is unambiguously determined even for a distance of 300 Mpc in the case of third-generation detectors.

DOI: [10.1103/PhysRevD.105.064063](https://doi.org/10.1103/PhysRevD.105.064063)

I. INTRODUCTION

Gravitational wave astronomy has entered a new era, characterized by the detection of a plethora of coalescing compact binary objects from the recent Advanced LIGO [1] and Advanced Virgo [2] runs [3–5], with a large range of masses for the individual compact objects. More detections are expected during the next observation period, called O4, with improved sensitivities and the inclusion of KAGRA [6]. In particular, the GW190814 event [7] corresponds to a merger involving a compact object with a 2.6 solar mass. Such a mass falls typically in the intermediate range between the known black hole masses and neutron star

masses [8–10], therefore this object can be either the most massive neutron star or the lightest black hole ever detected. In terms of gravitational wave emission, the main difference to be expected is the finite size effects in neutron stars. Unfortunately, the detector sensitivities are currently too low to constrain matter effects and the formation mechanism for a black hole or a neutron star of 2.6 solar masses remains unclear. An interesting idea is to consider that this object is a primordial black hole (PBHs) [11]. The GW190814 event is not the only event to contain a compact object of unknown nature because of a too low resolution of detectors; the question about the nature of compact objects can also be raised for the GW190425 event [12].

Contrary to stellar black holes which are produced by supernovae, PBHs may have been produced in the early Universe, during, e.g., a phase transition. Their size is limited by the Hubble scale, which is related to the cosmological time, providing a link between the maximum PBH mass and the epoch of formation [13]. In practice, PBHs can theoretically have a mass between the

*j-f.coupechoux@ipnl.in2p3.fr

Published by the American Physical Society under the terms of the [Creative Commons Attribution 4.0 International license](https://creativecommons.org/licenses/by/4.0/). Further distribution of this work must maintain attribution to the author(s) and the published article's title, journal citation, and DOI.

Planck mass and millions of solar masses. Because of Hawking evaporation, light PBHs lose mass under the form of radiation, and it has been shown that PBHs with masses below 10^{15} grams would have already evaporated since their formation [13]. On the contrary, heavier PBHs have a sufficiently low evaporation rate to still be present in our universe. Because of this, PBHs are usually considered as good candidates for dark matter [13], and can constitute the whole or a large fraction of it.

In the absence of an electromagnetic counterpart for a gravitational-wave signal, the nature of compact objects involved in a coalescence must be determined based solely on the gravitational waveforms. The data are compared to different models with Bayesian inference processes, and the preferred model is established based on the odds factor [14] which is equal to the Bayes factor without any *a priori* on the models. The effect of the structure of a neutron star on gravitational waveforms for the inspiral phase of a coalescence is described by a tidal deformability parameter [15–17] noted as Λ . This characterizes the quadrupole deformation of the star in response to the gravitational field of the companion.

The issue of compact objects identification based only on gravitational waveforms has been already studied in the literature. In [18], the Bayes factor is used on simulated data to differentiate between the hypothesis of a binary neutron star (BNS) and binary black hole (BBH) mergers. For data injected in Advanced LIGO, Virgo, and KAGRA (LVK) detectors in an O4-like configuration and with compact objects in the mass gap, the authors find that the distinction is possible only for binary systems within few tens of Mpc. This result is obtained assuming the APR [19] equation of state for neutron stars. More generally [20], the possibility to establish the nature of the compact object depends on the considered equation of state. Another study [21] investigates the possibility of distinguishing the nature of compact objects by analysing gravitational-wave signals from coalescences and assuming different equations of state. For high-mass injected binary neutron stars described by the ALF2 [22] and H4 [23,24] equations of state most BNS systems can be distinguished from BBH at 40 Mpc at a $\geq 95\%$ confidence level (CL) during the O4 LVK observation period. The study also suggests encouraging performance for third-generation detectors.

In this article, we study the difference between gravitational waveforms produced by the coalescence of BNS, BBH, and mixed systems containing a neutron star and a black hole (NSBH). The main goal is to understand under which circumstances and conditions it is possible to discriminate between BNS and BBH waveforms by making use of injected signals with realistic noise profiles. Section II introduces the tools used for comparing waveforms and to quantify how well different models describe the data. In Sec. III, we study the possibility of misinterpreting the results, when injecting either a BBH, or a BNS, or a NSBH

waveform into realistic detector noise, before concluding in Sec. IV.

II. MODEL SELECTION

A. Degeneracy between BNS, NSBH and BBH waveforms

The description of gravitational waveforms is achieved via the IMRPhenom family (phenomenological inspiral-merger-ringdown waveforms), which is based on frequency domain waveform models. In the following, the IMRPhenomPv2 [25–27] waveform approximant will be used for BBH, IMRPhenomPv2_NRTidal [28–30] for BNS and IMRPhenomNSBH [31] for NSBH.

It is important to notice that, in the specific case of BNS, for a given equation of state with an asymmetric system, the tidal deformabilities of the two neutron stars, Λ_1 and Λ_2 , are not the same. However, the parameter that is constrained at leading order by the gravitational-wave signal [32] is a combination of the tidal deformabilities of the two neutron stars, defined in [33] and noted $\tilde{\Lambda}$. For this reason, in the following BNS studies, we make the simplifying assumption $\Lambda_1 = \Lambda_2$.

1. Convolution product: A toy approach

A first approach to quantify the difference between two waveforms is to make their convolution product. This is defined by the time integral of the product of the two waveforms where one is time-shifted with respect to the other. By maximizing over the time shift, it is possible to have a measure of the similarity of two waveforms. The discriminating parameter to vary between the BNS, NSBH and BBH waveforms is the tidal deformability characterizing the matter effect [15–17]. Without mass gap hypothesis, it is this parameter that will play a central role in characterizing the nature of compact objects. The convolution product between a BBH and a BNS with a chirp mass of $1.44 M_\odot$ and a mass ratio of 0.9, normalized with the convolution product of the BBH with itself, is consistent with 1 for $\Lambda_1 = \Lambda_2 = 0$. This indicates that a neutron star with zero deformability mimics a black hole very well. By construction in this work, it is Λ that defines a neutron star and to get an idea of the order of magnitude of its effect, we have computed the value of the convolution product which gives a value of 0.959 for $\Lambda_1 = \Lambda_2 = 300$, and of 0.934 for $\Lambda_1 = \Lambda_2 = 600$.

2. Match between two waveforms

The comparison of gravitational waveforms using the convolution product does not take into account the ability to experimentally measure a difference with an interferometer. Following Ref. [34], the approach to compare two waveforms taking into account the sensitivity of the detectors is based on the noise-weighted inner product between two waveforms h_1 and h_2 defined by:

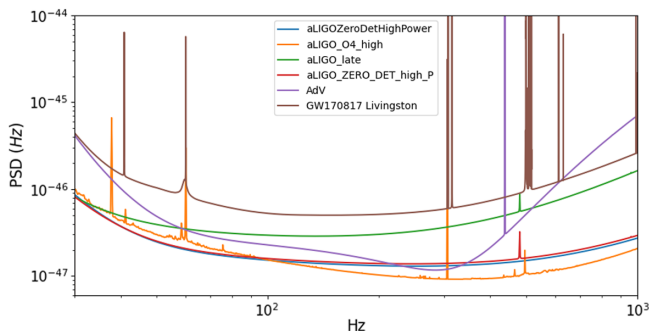


FIG. 1. Noise power spectral densities considered in this study. In brown the PSD of LIGO Livingston at the time of GW170817 and in blue the PSD design sensitivity of Advanced LIGO available in the `psd` package within `pyCBC` [36]. The other curves correspond to a PSD design sensitivity for different scenarios of Advanced LIGO and Advanced Virgo available in the detector package within `Bilby` [38].

$$\langle h_1 | h_2 \rangle = 4 \operatorname{Re} \int_{f_{\min}}^{f_{\max}} \frac{h_1(f) h_2^*(f)}{S_n(f)} df, \quad (1)$$

where $S_n(f)$ is the power spectral density (PSD), that encodes the frequency-dependent sensitivity of a detector [35]. To calculate such a scalar product, we take the advanced LIGO design sensitivity given by `aLIGOZeroDetHighPower` [36], shown in Fig. 1. The figure also shows the PSD of LIGO Livingston at the time of the GW170817 detection, illustrating that the sensitivity used in our study is roughly one order of magnitude better than the best performance of the detectors during the O2 run [3]. The separation between two waveforms h_1 and h_2 can be related to their match, which is defined by the overlap maximized on the coalescence time and the coalescence phase:

$$M(h_1, h_2) = \max_{\Delta t, \Delta \phi} \frac{\langle h_1 | h_2 \rangle}{\sqrt{\langle h_1 | h_1 \rangle} \sqrt{\langle h_2 | h_2 \rangle}}. \quad (2)$$

To detect gravitational-wave signals from compact binary coalescences (CBC), the LIGO-Virgo Collaboration (LVC) constructs template banks so that the match is at least 0.97 between the two closest waveforms [37]. Matter effects on gravitational waveforms, needed to determine the nature of compact objects, can be very small. As an example, considering a BBH and a BNS both with a chirp mass of $1.44 M_\odot$ and a mass ratio of 0.9, the tidal deformabilities of the neutron stars must be at least of the order of $\Lambda_1 = \Lambda_2 = 800$ to have a match lower than 0.97.

3. Results with confidence regions

When a signal is detected, given a model \mathcal{M}_A , the marginalized posterior probability density function of all unknown parameters θ is typically computed by using a

Bayesian analysis. The mean of the parameters θ is noted $\langle \theta \rangle$. Following Eq. (18) of [39], the confidence region at a given probability p is the set of points verifying the following condition:

$$2\rho^2[1 - M(h(\theta), h(\langle \theta \rangle))] \leq \chi_k^2(1 - p), \quad (3)$$

where ρ is the signal to noise ratio (SNR) and $\chi_k^2(1 - p)$ is the value of the quantile function for the normal chi-squared distribution corresponding to p , in the case of k degrees of freedom. We can use this relation to determine the regions in the parameter space in which two different waveforms can be distinguished. For a given SNR, if spins are neglected, BNS templates have only 4 parameters: the chirp mass \mathcal{M} , the mass ratio q and the two tidal deformabilities Λ_1 , Λ_2 because the match is maximized over phase, time, and distance.

We consider only the tidal deformabilities as free parameters and fix the others. This assumption neglects the degeneracies between the parameters of a waveform (see for example [39]) leading to possibly optimistic results. In addition, as explained, we make the simplifying assumption that $\Lambda_1 = \Lambda_2$. We write Eq. (3) for the case where $h(\langle \theta \rangle)$ is a BBH waveform and for the case where $h(\theta)$ is a BNS one with $\Lambda_1 = \Lambda_2$. It follows that BBH and BNS can be distinguished (and the nature of the compact object can be determined) if:

$$2\rho^2[1 - M(h_{\text{BNS}}, h_{\text{BBH}})] \geq \chi_k^2(1 - p). \quad (4)$$

Since the tidal deformability is the only degree of freedom ($\Lambda_1 = \Lambda_2$), the value of the quantile function for the normal chi-squared distribution $\chi_{k=1}^2(1 - p)$ is equal to 2.71 for $p = 0.1$, which corresponds to a 90% CL and 6.64 for $p = 0.01$, which corresponds to a 99% CL.

The left-hand side of Eq. (4) depends on the fixed parameters but also on the luminosity distance d through the SNR: $\rho \simeq \langle h_{\text{BBH}} | h_{\text{BBH}} \rangle^{1/2} \simeq \langle h_{\text{BNS}} | h_{\text{BNS}} \rangle^{1/2}$ which is proportional to $1/d$. Figure 2 shows $2\rho^2[1 - M(h_{\text{BNS}}, h_{\text{BBH}})]$ as a function of the deformability of neutron stars. The horizontal lines correspond to the 90% and 99% CL limits: a point above one of these lines means that BBH and BNS mergers can be distinguished at more than 90% of 99% CL. As expected, the ability of distinguishing BBH and BNS (all other parameters being fixed) increases with the tidal deformabilities and the chirp mass, and decreases with the distances. For example, for a distance of $d = 200$ Mpc, with $\mathcal{M} = 1.44 M_\odot$ and $q = 0.9$, the nature of the compact objects can be determined if the tidal deformabilities are higher than 200, while for a distance of 400 Mpc even tidal deformabilities of 1000 are not enough to make the BBH and BNS waveforms distinguishable at 99% CL. It has to be kept in mind that, for most equations of state, a higher mass typically implies a lower deformability. For example, considering

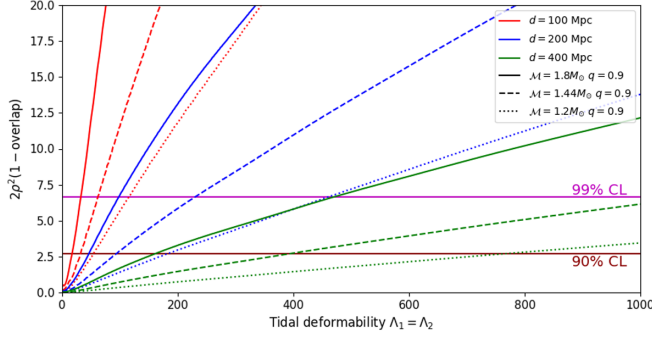


FIG. 2. Comparison between BBH and BNS waveforms. The curves show the left-hand side of Eq. (4) as a function of the tidal deformabilities of the neutron stars. The horizontal lines show the value of χ^2_k for different confidence level thresholds: if a point is below the horizontal lines, the two mergers are too similar to be distinguished at the given confidence level. Different types of curves (solid, dashed, and dotted) of the same color indicate different chirp masses and different types of colors indicate different distances. In particular, ($\mathcal{M} = 1.2 M_\odot, q = 0.9$) corresponds to ($m_1 = 1.45 M_\odot, m_2 = 1.31 M_\odot$), ($\mathcal{M} = 1.44 M_\odot, q = 0.9$) to ($m_1 = 1.74 M_\odot, m_2 = 1.57 M_\odot$) and ($\mathcal{M} = 1.8 M_\odot, q = 0.9$) to ($m_1 = 2.18 M_\odot, m_2 = 1.96 M_\odot$).

the APR equation of state, a $1.655 M_\odot$ neutron star has a tidal deformability of 135 which is in the region between 90% CL and 99% CL (see blue dashed curve of Fig. 2). However, a neutron star of $2.07 M_\odot$ has a tidal deformability lower than 46 which is below 90% CL (see blue solid curve of Fig. 2).

We performed a similar study for the comparison of BBH and NSBH waveforms, to determine the conditions under which it is possible to distinguish the nature of the compact object coalescing with the BH. The results are presented in Fig. 3 for a system with a chirp mass of $3 M_\odot$ and assuming different mass asymmetries. The case of extreme mass ratio ($q = 0.6$) is at the edge of the standard parameter space, with a NS of $2.7 M_\odot$ and a BH of $4.5 M_\odot$. At fixed tidal deformability, the distinction between BBH and NSBH is

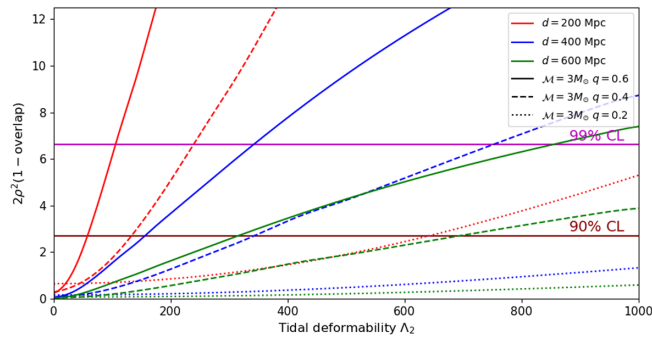


FIG. 3. Same as Fig. 2 for BBH and NSBH templates. ($\mathcal{M} = 3 M_\odot, q = 0.2$) corresponds to ($m_1 = 8.2 M_\odot, m_2 = 1.6 M_\odot$), ($\mathcal{M} = 3 M_\odot, q = 0.4$) to ($m_1 = 5.6 M_\odot, m_2 = 2.2 M_\odot$) and ($\mathcal{M} = 3 M_\odot, q = 0.6$) to ($m_1 = 4.5 M_\odot, m_2 = 2.7 M_\odot$).

more difficult at low mass ratios. For a chirp mass of $3 M_\odot$, a mass ratio of 0.2, a tidal deformability of 650, the system must be at a distance of less than 200 Mpc to know the nature of the second compact object at 90% CL. By construction, when the deformability is zero, the waveforms used do not make it possible to distinguish between a BH and a NS. Indeed, in this case, the overlap is above 0.99 and consistent with 1 within the model precision, as described in [31]. However the y axis of Fig. 3 combines the overlap with the SNR (ρ), leading to nonexactly zero values of the curves at null tidal deformabilities for the loudest coalescences, for which the modeling error would dominate the comparison of the waveforms.

The results shown in Figs. 2 and 3 depend strongly on the detector sensitivity. Indeed, any change in the PSD $S_n(f)$ directly affects the noise-weighted inner product between two waveforms [Eq. (1)]. Some examples of PSD are drawn in Fig. 1. Their impact on the ability to distinguish between BBH and BNS templates and to determine the nature of compact objects is shown in Fig. 4 for the system defined by $\mathcal{M} = 1.44 M_\odot, q = 0.9$ and $d = 200$ Mpc.

B. The odds number

The Bayes' theorem links the posterior distribution to the likelihood, the prior and the evidence [14]:

$$p(\theta|d, \mathcal{M}_A) = \frac{\pi(\theta|\mathcal{M}_A)\mathcal{L}(d|\theta, \mathcal{M}_A)}{\mathcal{Z}(d|\mathcal{M}_A)}, \quad (5)$$

$p(\theta|d, \mathcal{M}_A)$ is the posterior distribution which gives the probability of all unknown parameters θ , given the experimental data d within the model \mathcal{M}_A . $\mathcal{L}(d|\theta, \mathcal{M}_A)$ is the likelihood function. $\pi(\theta|\mathcal{M}_A)$ is the prior assuming \mathcal{M}_A . $\mathcal{Z}(d|\mathcal{M}_A)$ is the evidence which is the integral over the full set of parameters θ of the product of the likelihood and the prior:

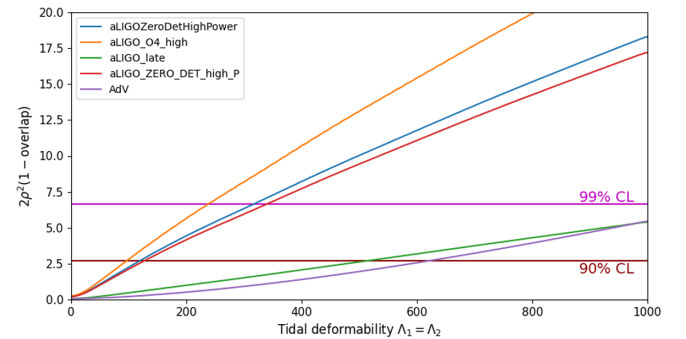


FIG. 4. Comparison between BBH and BNS mergers, assuming the different power spectral densities shown in Fig. 1. The chirp mass is fixed at $1.44 M_\odot$, the mass ratio at 0.9 and the distance at 200 Mpc.

TABLE I. Jeffrey’s scale standard values used to compare two competing models using the Bayes factor.

$ \ln \mathcal{B}_{AB} $	Probability	
< 1	< 0.731	Inconclusive
2.5	0.924	Moderate evidence
5	0.993	Strong evidence

$$\mathcal{Z}(d|\mathcal{M}_A) = \int d\theta \mathcal{L}(d|\theta, \mathcal{M}_A) \pi(\theta|\mathcal{M}_A). \quad (6)$$

Our goal is to study when BNS, NSBH and BBH mergers can be distinguished via the waveforms of the emitted gravitational waves. Bayesian analysis estimates the posterior probability density function for a given model \mathcal{M}_A . In order to compare two competing models, the odds number can be used [14]:

$$\mathcal{B}_{AB} = \frac{p(\mathcal{M}_A|d)}{p(\mathcal{M}_B|d)} = \frac{p(\mathcal{M}_A) \mathcal{Z}_A}{p(\mathcal{M}_B) \mathcal{Z}_B}, \quad (7)$$

where $\mathcal{Z}_{A/B}$ is the evidence and $p(\mathcal{M}_{A/B})$ is the prior belief in model A/B . Thereafter, gravitational-wave data are analyzed without assumption on the nature of the compact objects whichever their mass, and $p(\mathcal{M}_A)/p(\mathcal{M}_B)$ is fixed to one. $\mathcal{B}_{AB} = \mathcal{Z}_A/\mathcal{Z}_B$ is the Bayes factor between the two competing models \mathcal{M}_A and \mathcal{M}_B . Jeffrey’s scale [40] gives an empirical calibration of the strength of evidence and if $\ln \mathcal{B}_{AB}$ is higher than the arbitrary value of 5, \mathcal{M}_A is strongly preferred. Limits for strong evidence, moderate evidence and inconclusive are given in Table I.

It is important to notice that a Bayes factor penalizes more complicated models with a large prior volume or a fine tuning. In other words, a particularly simple model giving a worse fit to the data can be preferred over a complicated model giving a better fit. This can be intuitively understood invoking the Occam’s razor principle as explained in Ref. [41].

III. MODEL COMPARISON WITH BAYES FACTOR IN SIMULATED DATA

In this section the templates (generated with IMRPhenomPv2, IMRPhenomPv2_NRTidal and IMRPhenomNSBH to describe BBH, BNS and NSBH waveforms, respectively) are used to analyze LVC simulated data. We perform a Bayesian analysis for each template and study the output in terms of the posterior distribution of the parameters and the signal-to-noise ratio. To determine which template better describes the data, we use the odds number introduced in the previous section. The power spectral density of the detector noise is taken to be the one of the advanced configurations for the O4 simulations [42]. The analysis is performed in the case where the

simulated signal corresponds to a BBH, BNS, or NSBH system. Each time, the Bayes factor between the three corresponding models is computed in order to find which one describes best the simulated data, with a decisive choice whenever the Bayes factor is higher than 5. The results are obtained using pBilby [38,43,44] with nested sampling, as introduced by Skilling [45].

A. Injected waveform

The first step in this study consists in generating a gravitational waveform given by a template and adding it to the design Gaussian noise of advanced detector configurations as reported in [46]. The gravitational waveform depends on 15 parameters: chirp mass \mathcal{M} , mass ratio q , two angular momenta $\vec{S}_{1,2}$ (for aligned spin systems, only $\chi_i = \vec{S}_i \cdot \hat{L}/m_i^2$ are needed, where \hat{L} is the normalized orbital momentum), 2-dimensional sky localization (right ascension ra and declination dec), luminosity distance d , two angles for the orbital plane (inclination angle ι and the polarization angle ψ), coalescence time t and phase of coalescence ϕ . For a BNS merger, 17 parameters must be used because the two tidal deformabilities Λ_1 and Λ_2 must be added to the list.

The location of the source in the sky is arbitrarily chosen to maximize the signal for the second most sensitive detector. The PSD for the Virgo detector, which determines the sensitivity of the detector, is chosen for the advanced configuration, shown in purple in Fig. 1. For the Hanford and Livingston detectors, the PSD has been represented in orange and is the same for both. The source location is taken to maximize the signal for the Hanford detector. For a coalescence at a GPS time of 1.2×10^9 s, this gives 5.49 rad for right ascension and 0.81 rad for declination. The inclination and polarization are chosen at 0 rad. For a physical luminosity distance of 400 Mpc, the effective distance for these parameters gives 400 Mpc for Hanford, 449 Mpc for Livingston, and 1867 Mpc for Virgo.

The spin of neutron stars in a binary system is generally extremely weak. Well before the inspiral phase detected by gravitational-wave detectors, the spin of neutron stars is suppressed by electromagnetic interactions. On the contrary, standard and primordial black holes, which do not have this suppression mechanism, can have larger spins during the merger, and a primordial black hole can even have a spin very close to that of an extreme Kerr black hole. If a compact object is detected with a large spin, there is a strong chance that it is a black hole and if the spin is almost equal to 1, a primordial black hole. *A priori* though, it is always possible to assume a spinning NS, and the presence of a spinning black hole in the coalescence will not necessarily increase the odds number to distinguish two models. As for the mass criterion, we propose here to study the distinction between black hole and neutron star only with the Bayes factor without adding assumptions in the

prior and we will restrict ourselves to compact objects injected without spin.

In the following, we will consider an injected signal with the optimal configuration for Hanford as described in above. Compact objects are chosen without spin and with masses equal to $m_1 = 1.74 M_\odot$ and $m_2 = 1.57 M_\odot$ i.e., a chirp mass of $\mathcal{M} = 1.44 M_\odot$ with $q = 0.9$ and $\chi_i = 0$. For an injected BBH data created by IMRPhenomPv2 routine, only the luminosity distance varies between the different injections. For BNS data created by the IMRPhenomPv2_NRTidal routine, the luminosity distance and the tidal deformabilities will be varied.

B. Black hole mergers interpreted as neutron star mergers

The Bayes factor is calculated between BBH/NSBH models and BBH/BNS models for an injected BBH signal of 128 seconds as described in the previous section. The sampling parameters used for the Bayesian analysis, performed using parallel bilby are given in Table II. The full set of parameters is investigated: there are 11 parameters for BBH, 12 parameters for NSBH, and 13 parameters for BNS. The Bayes factor depends on the template but also on the prior. To reduce the dependence on the prior, the same is used for a BBH and for a BNS, namely we use a uniform prior between $0.87 M_\odot$ and $5 M_\odot$ for the chirp mass and between 0.125 and 1 for the mass ratio with constraints $1 M_\odot < m_1 < 5 M_\odot$ and $1 M_\odot < m_2 < 3 M_\odot$ for all the models. We also use aligned spins in the low spin limit corresponding to $|\chi_i| < 0.05$ for each model. Only the tidal deformability, modeling the matter effects for a NS, has no correspondent for a BH. In this case, a uniform prior between 0 and 5000 for Λ is added for a NS.

Figure 5 shows the variation of the Bayes factor as a function of the distance. In all cases the values of $\ln \mathcal{B}_{AB}$ represented by the dots are positive, meaning that the \mathcal{M}_A model is always preferred. If a point is above the dashed horizontal line, the \mathcal{M}_A model is *strongly* better (cf. Table I). The \mathcal{M}_A model corresponds to a BBH merger, i.e., the

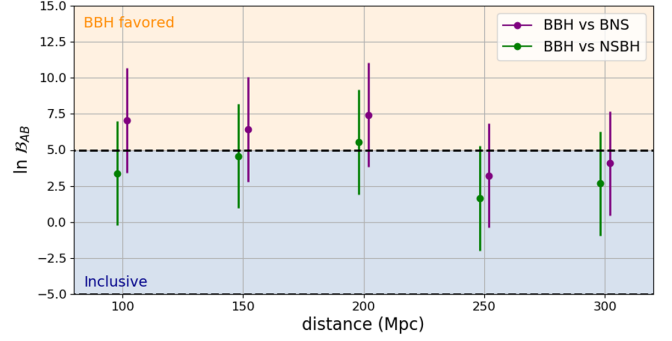


FIG. 5. Bayes factor for different models as a function of the luminosity distance for the optimal configuration. The chirp mass of BBH injected data is chosen to be $1.44 M_\odot$ with a mass ratio of 0.9 and the sampling parameters for BBH, NSBH and BNS are given in Table II. A point above the dashed black lines means that the BBH hypothesis is strongly favored. In the blue region labeled “Inclusive” it is not possible to strongly prefer one model over the other.

model which corresponds to the BBH injected signal, and the \mathcal{M}_B model corresponds either to a BNS merger or to a NSBH merger. For a distance smaller than 200 Mpc, the purple dots in Fig. 5 are in the orange region and the BBH model is preferred over the BNS model which is not really the case for the NSBH model (green dots). We can therefore conclude that there is at least one black hole in the source that emitted the gravitational waves. The BNS waveform with almost zero tidal deformability fits very well with the BBH waveform, so the Bayes factor will prefer the model with the smallest number of parameters and as expected, the purple dots are above the green dots and above zero. Each dot plotted in Fig. 5 is the result of one or two independent Bayesian analyses and is accompanied by a vertical bar corresponding to the possible variation of the result: this bar represents the uncertainty of the Bayes factor and its variation due to different realizations of the noise. This uncertainty has been estimated with eight simulations in the zone where a model is strongly favored ($d = 150$ Mpc) and in the inclusive zone ($d = 300$ Mpc). Later in the

TABLE II. Sampling parameters used for the different Bayesian analyses. The parameters not mentioned in sampling parameters are set to the value used in the injected data.

	Name of models	Number	Sampling parameters
Restricted space	BBH W/O spin	2	\mathcal{M}, q
	BNS W/O spin	4	$\mathcal{M}, q, \Lambda_1, \Lambda_2$
	BBH 1D spin	4	$\mathcal{M}, q, \chi_1, \chi_2$ (aligned spin)
	BBH 3D spin	8	$\mathcal{M}, q, a_1, a_2, \theta_1, \theta_2, \phi_{JL}, \phi_{12}$ (full spin description)
	BNS W/O spin with Λ_i fixed	2	\mathcal{M}, q (Λ_1 and Λ_2 are fixed at 0)
Full space	BBH	11	$\mathcal{M}, q, \chi_1, \chi_2, ra, dec, d, \theta_{JN}, \psi, t, \phi$
	NSBH	12	$\mathcal{M}, q, \chi_1, \chi_2, \Lambda_2, ra, dec, d, \theta_{JN}, \psi, t, \phi$
	BNS	13	$\mathcal{M}, q, \chi_1, \chi_2, \Lambda_1, \Lambda_2, ra, dec, d, \theta_{JN}, \psi, t, \phi$
	BNS with Λ_i fixed	11	$\mathcal{M}, q, \chi_1, \chi_2, ra, dec, d, \theta_{JN}, \psi, t, \phi$ ($\Lambda_1 = \Lambda_2 = const$)

manuscript (Fig. 7), we show those simulation points. When the odds number is close to the limit of 5 it is not always possible to discriminate between the BBH and BNS models even with a source at a distance of 100 Mpc.

In this section and in the following we have assumed the source as oriented favorably for detection and the results are therefore rather optimistic. Moreover, we have considered a Gaussian noise for the detectors without considering terrestrial noise due for instance to meteorological conditions or human activity which is an ideal case. On the other hand, the limit can slightly improve with the increase of the chirp mass.

C. Neutron star mergers interpreted as black hole mergers

In this section, we consider the case where the injected data are generated by mergers of BNS and we try to determine whether it is possible to confuse a BNS merger with nonzero tidal deformability with a BBH merger. We inject the gravitational waveforms generated by mergers of BNS with different tidal deformabilities and zero spin at different distances and study the Bayes factor between BNS and BBH.

1. Study on spin in restricted parameter space

First, we focus on the impact of the black hole spins on the Bayes factor. In order to reduce the computational cost, only the physical parameters of the objects are searched for, using a Bayesian analysis. The sampling parameters for the different models considered are given in Table II and the results are shown in Fig. 6. In the top panel, the Bayes factor is calculated between the BNS without spin model and a BBH model with different spin descriptions defined in Table II. For data injected with $\Lambda_1 = \Lambda_2 = 600$ or with $\Lambda_1 = \Lambda_2 = 300$, the BNS without spin model is always preferred regardless of the BBH models. For data injected with $\Lambda_1 = \Lambda_2 = 100$, the most favored case is the BBH without spin model. Not taking spin into account in the BBH analysis, a BBH is unable to mimic a BNS and the posterior distribution of the mass ratio is not compatible with the injected value of 0.9. The spin description allows for an improved signal fit with the BBH model due to the flexibility provided by a larger parameter space. On the other hand, the Bayes factor will not automatically be better because it penalizes models with a larger number of parameters, as shown by the blue and red dots, and using a 3D spin description is worse than a 1D description within the BBH model. For data injected with $\Lambda_1 = \Lambda_2 = 100$, some values of $\ln \mathcal{B}_{AB}$ slightly prefer the BBH model in spite of the fact that the signal was created with a BNS model. The bottom panel of Fig. 6 shows a new Bayesian analysis with the model BNS without spin with Λ_i fixed represented with black dots. In this case, the BBH model is no longer preferred compared to the BNS model.

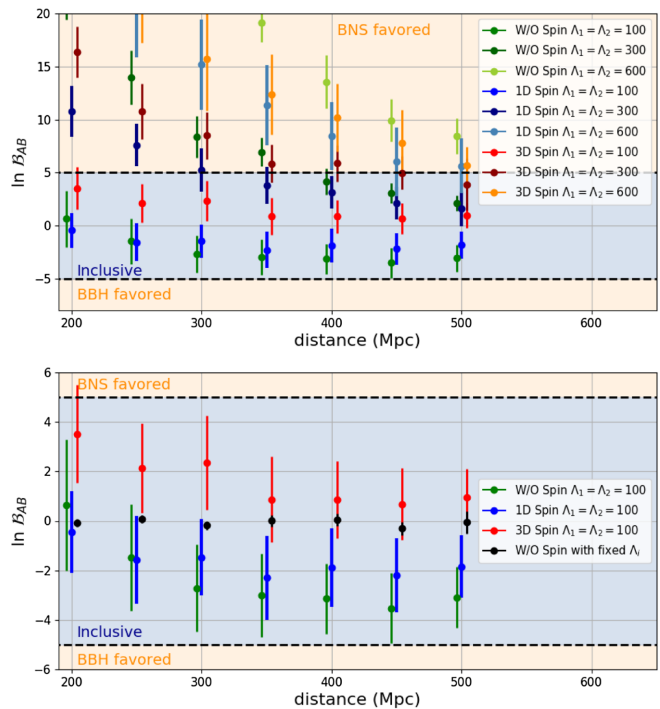


FIG. 6. Top panel: Bayes factor in restricted space between the model called BNS without spin and different models of BBH as a function of the luminosity distance. The sampling parameters corresponding to the different models are given in Table II and the injected data correspond to BNS mergers in optimal configuration and with zero spins. Each point represents the mean value and the vertical bar the standard deviation for 4 to 6 simulations with different noise realizations. A dot located in the orange regions means that one of the two analyses is strongly preferred by the data. Bottom panel: zoom on the results for an injection with $\Lambda_1 = \Lambda_2 = 100$. The black points are added and correspond to the Bayesian analysis performed with BNS without Spin with Λ_i fixed and with BBH without Spin (see Table II).

2. Full space parameters

In this section, the complete parameter space is probed via a Bayesian analysis (see Table II) for the same injected data as in Fig. 6. The Bayes factor between BNS and BBH is shown in Fig. 7. As expected, the larger the tidal deformability, the clearer the distinction and the less a BBH merger can mimic a BNS merger. We can also notice the strong impact of the distance from the source on the results. When $d = 100$ Mpc, the tidal deformability is clearly reconstructed if $\Lambda_1 = \Lambda_2 \geq 300$. For a distance around 200 Mpc, the Bayes factor is not systematically in the orange region even for a strong tidal deformability and for a distance of 300 Mpc, it is no longer possible to discriminate the nature of the compact objects.

When the injected signal is a BBH (see Fig. 5), the Bayesian analysis never prefers the BNS model even if it is not possible to conclude that it is a BBH because the Bayes factor does not reach the strong evidence limit. The purple dots in Fig. 7, which correspond to a BNS signal

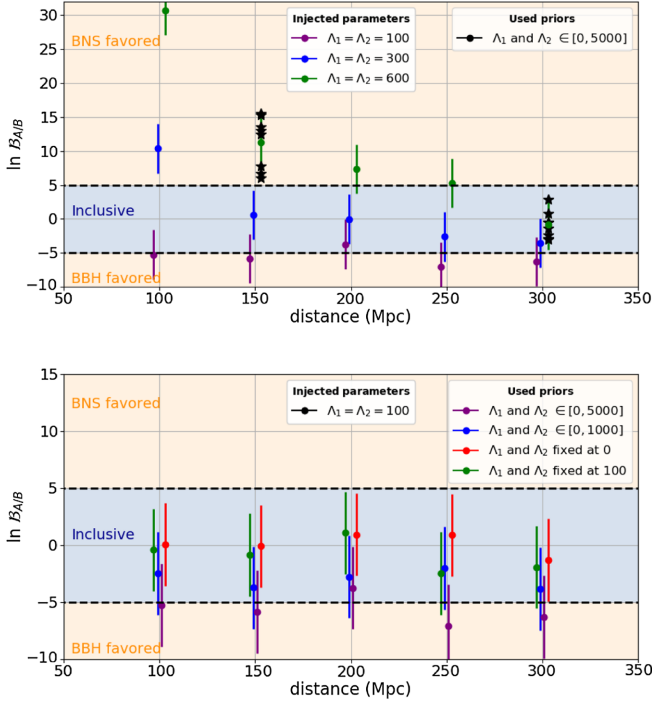


FIG. 7. Bayes factor in the full space between BNS and BBH models as a function of the luminosity distance for different tidal deformabilities. The sampling parameters corresponding to the different models are given in Table II and the injected data are the same as in Fig. 6. A point in the orange regions means that one of the two models is preferred, whereas a point in the blue region corresponds to an inconclusive discrimination of the best model. The variation of the results using different realizations of the noise is represented by the black stars, which were used to draw the vertical bars. Top panel: Results showing the variation of the Bayes factor for data injected with different deformabilities. The analysis is performed using the so-called BNS model. Bottom panel: Results showing the variation of the Bayes factor for an analysis using different choices of priors with the BNS model and BNS with Λ_i fixed. The analysis is performed using the same data injected with neutron stars having tidal deformabilities equal to 100.

with $\Lambda_1 = \Lambda_2 = 100$, seem to suggest that the BBH merger is preferred over the BNS one. This preference is a manifestation of the fact that the BNS model is more complex than the BBH model, having two additional parameters. This is demonstrated by the bottom panel in Fig. 7, which analyzes the same data with different priors. When the analysis is performed with a BNS waveform having the tidal deformabilities fixed to zero (BNS with Λ_i fixed at zero), the Bayes factor is fully consistent with zero (red dots). This result is not surprising as the BBH waveform and the BNS waveform with zero tidal deformability are almost identical. However, there is no improvement in the Bayes factor if the tidal deformability is set to 100, i.e., to the value that was used to create the injected data. The preference for a BBH hypothesis increases from Λ constant to Λ in $[0, 1000]$ and $[0, 5000]$ because of the

increasing volume of the prior. Considering the PSD of the advanced detector configurations, the Bayes factor does not distinguish between the BNS model and the BBH model when the source is at 300 Mpc even in the case where the tidal deformabilities are large ($\Lambda_1 = \Lambda_2 = 600$).

A significant improvement is expected with third generation detectors, for instance Einstein Telescope [47]. To have an idea of this improvement, BNS signals with $\Lambda_1 = \Lambda_2 = 100$ and $\Lambda_1 = \Lambda_2 = 600$ are injected at a distance of 300 Mpc in the Hanford detector with the PSD [48] of Einstein Telescope and in the Livingston detector with the PSD of the advanced detector configuration. For $\Lambda_1 = \Lambda_2 = 100$, the Bayes factor is now consistent with zero, improving the situation of the advanced detectors configuration only, when the BBH model was slightly preferred. On the other hand, for a BNS signal with $\Lambda_1 = \Lambda_2 = 600$, the Bayes factor becomes now 90, meaning that the BNS model is strongly favored compared to the BBH model. In the advanced detectors configuration the factor was consistent with zero, implying an inconclusive determination of the nature of the compact object.

IV. CONCLUSIONS

The nature of the compact $2.6 M_\odot$ object detected in the GW190814 event is unknown: is it a neutron star, a black hole, a new type of compact object? Motivated by this event, we studied how a gravitational waveform of a BBH merger can be distinguished from a BNS merger. The distinction between BNS and BBH is typically made by considering that there is a mass gap between black holes and neutron stars: a neutron star has a mass lower than $2.2 M_\odot$ and a stellar black hole higher than $5 M_\odot$. The problem with the observed object at $2.6 M_\odot$ is that it does not fit into this classification. On the contrary, if primordial black holes exist, they may have masses similar to neutron stars. This is why it is important to study the distinction between a black hole and a neutron star by considering only the gravitational waveform without priors on the mass distributions.

As a first step, we have compared waveforms from BBH, BNS, and NSBH templates by using the match function defined in Eq. (2). From this study, even for large neutron star tidal deformabilities, the observation of gravitational waves from a merger at 400 Mpc appears not to be enough to identify a BNS signal. We have also observed that, for an asymmetric NSBH merger, the identification of the second compact object via its tidal deformability is more difficult than in the case of BNS, even considering a chirp mass of $3 M_\odot$.

In a second step, we have studied simulated data as it is done in real gravitational wave analyses, where the parameters of a merger are determined with Bayesian inference. A selection criterion for the nature of the coalescence is given by the ratio of the Bayes factors between two competing models. We have studied this ratio for simulated data under

realistic noise conditions by considering mergers with a chirp mass of $1.44 M_{\odot}$. For BBH simulated data, the BBH models are preferred at least up to a distance of 300 Mpc. For BNS simulated data with $\Lambda_1 = \Lambda_2 = 600$, BNS models are largely favored over BBH. On the other hand, when $\Lambda_1 = \Lambda_2 = 100$, the BBH model is preferred. This is due to the fact that the Bayes factor depends on the prior volume and penalizes more complex systems with a larger number of parameters. We have checked that a tighter cut on the Bayes factor ratio can avoid this situation.

The detection of a BNS merger at a distance larger than 150 Mpc does not have a signal to noise ratio good enough to allow the determination of the nature of compact objects, even if the merger is perfectly oriented for the Hanford detector, assuming design sensitivities and only stationary

noise. Considering third generation detectors, for instance Einstein Telescope, and under the same optimistic assumptions as before, the ability to distinguish between two models is dramatically improved.

ACKNOWLEDGMENTS

This work is supported by the STRONG-2020 network from the European Union’s Horizon 2020 research and innovation program under Grant agreement No. 824093 (H. H.); the Laboratoire d’Excellence (LABEX) Lyon Institute of Origins (ANR-10-LABX-0066) of the Université de Lyon for its financial support within the program “Investissements d’Avenir” (ANR-11-IDEX-0007) of the French government operated by the National Research Agency.

-
- [1] J. Aasi *et al.* (LIGO Scientific Collaboration), *Classical Quantum Gravity* **32**, 074001 (2015).
- [2] F. Acernese *et al.* (Virgo Collaboration), *Classical Quantum Gravity* **32**, 024001 (2015).
- [3] B. Abbott *et al.* (LIGO Scientific, Virgo Collaborations), *Phys. Rev. X* **9**, 031040 (2019).
- [4] R. Abbott *et al.* (LIGO Scientific, Virgo Collaborations), *Phys. Rev. X* **11**, 021053 (2021).
- [5] R. Abbott *et al.* (LIGO Scientific, Virgo, KAGRA Collaborations), [arXiv:2111.03606](https://arxiv.org/abs/2111.03606) [*Phys. Rev. X* (to be published)].
- [6] T. Akutsu *et al.* (KAGRA Collaboration), *Prog. Theor. Exp. Phys.* **2021**, 05A101 (2021).
- [7] R. Abbott *et al.* (LIGO Scientific, Virgo Collaborations), *Astrophys. J. Lett.* **896**, L44 (2020).
- [8] L. Rezzolla, E. R. Most, and L. R. Weih, *Astrophys. J.* **852**, L25 (2018).
- [9] B. P. Abbott *et al.* (LIGO Scientific, Virgo Collaborations), *Classical Quantum Gravity* **37**, 045006 (2020).
- [10] O. Pejcha and T. A. Thompson, *Astrophys. J.* **801**, 90 (2015).
- [11] C. T. Byrnes, M. Hindmarsh, S. Young, and M. R. S. Hawkins, *J. Cosmol. Astropart. Phys.* **08** (2018) 041.
- [12] B. Abbott *et al.* (LIGO Scientific, Virgo Collaborations), *Astrophys. J. Lett.* **892**, L3 (2020).
- [13] B. Carr and F. Kuhnel, *Annu. Rev. Nucl. Part. Sci.* **70**, 355 (2020).
- [14] E. Thrane and C. Talbot, *Pub. Astron. Soc. Aust.* **36**, e010 (2019).
- [15] E. E. Flanagan and T. Hinderer, *Phys. Rev. D* **77**, 021502 (2008).
- [16] T. Hinderer, *Astrophys. J.* **677**, 1216 (2008).
- [17] T. Hinderer, *Astrophys. J.* **697**, 964 (2009).
- [18] S. Datta, K. S. Phukon, and S. Bose, *Phys. Rev. D* **104**, 084006 (2021).
- [19] A. Akmal, V. R. Pandharipande, and D. G. Ravenhall, *Phys. Rev. C* **58**, 1804 (1998).
- [20] T. Hinderer, B. D. Lackey, R. N. Lang, and J. S. Read, *Phys. Rev. D* **81**, 123016 (2010).
- [21] A. Chen, N. K. Johnson-McDaniel, T. Dietrich, and R. Dudi, *Phys. Rev. D* **101**, 103008 (2020).
- [22] M. Alford, M. Braby, M. W. Paris, and S. Reddy, *Astrophys. J.* **629**, 969 (2005).
- [23] B. D. Lackey, M. Nayyar, and B. J. Owen, *Phys. Rev. D* **73**, 024021 (2006).
- [24] N. K. Glendenning, *Astrophys. J.* **293**, 470 (1985).
- [25] S. Husa, S. Khan, M. Hannam, M. Pürrer, F. Ohme, X. Jiménez Forteza, and A. Bohé, *Phys. Rev. D* **93**, 044006 (2016).
- [26] S. Khan, S. Husa, M. Hannam, F. Ohme, M. Pürrer, X. Jiménez Forteza, and A. Bohé, *Phys. Rev. D* **93**, 044007 (2016).
- [27] S. Khan, K. Chatziioannou, M. Hannam, and F. Ohme, *Phys. Rev. D* **100**, 024059 (2019).
- [28] T. Dietrich, S. Bernuzzi, and W. Tichy, *Phys. Rev. D* **96**, 121501 (2017).
- [29] T. Dietrich *et al.*, *Phys. Rev. D* **99**, 024029 (2019).
- [30] T. Dietrich, A. Samajdar, S. Khan, N. K. Johnson-McDaniel, R. Dudi, and W. Tichy, *Phys. Rev. D* **100**, 044003 (2019).
- [31] J. E. Thompson, E. Fauchon-Jones, S. Khan, E. Nitoglia, F. Pannarale, T. Dietrich, and M. Hannam, *Phys. Rev. D* **101**, 124059 (2020).
- [32] T. Damour, A. Nagar, and L. Villain, *Phys. Rev. D* **85**, 123007 (2012).
- [33] L. Wade, J. D. E. Creighton, E. Ochsner, B. D. Lackey, B. F. Farr, T. B. Littenberg, and V. Raymond, *Phys. Rev. D* **89**, 103012 (2014).
- [34] L. Lindblom, B. J. Owen, and D. A. Brown, *Phys. Rev. D* **78**, 124020 (2008).
- [35] C. Cutler and E. E. Flanagan, *Phys. Rev. D* **49**, 2658 (1994).
- [36] A. Nitz *et al.*, gwastro/pycbc: 1.18.0 release of pycbc (2021).

- [37] S. Babak, R. Balasubramanian, D. Churches, T. Cokelaer, and B. S. Sathyaprakash, *Classical Quantum Gravity* **23**, 5477 (2006).
- [38] G. Ashton *et al.*, *Astrophys. J. Suppl. Ser.* **241**, 27 (2019).
- [39] E. Baird, S. Fairhurst, M. Hannam, and P. Murphy, *Phys. Rev. D* **87**, 024035 (2013).
- [40] H. Jeffreys, *Theory of Probability* (Oxford University Press, USA, 1961).
- [41] D. J. C. MacKay, *Information Theory, Inference and Learning Algorithms* (Cambridge University Press, USA, 2002).
- [42] LIGO Document T2000012-v1, <https://dcc.ligo.org/LIGO-T2000012/public>.
- [43] I. M. Romero-Shaw *et al.*, *Mon. Not. R. Astron. Soc.* **499**, 3295 (2020).
- [44] R. J. E. Smith, G. Ashton, A. Vajpeyi, and C. Talbot, *Mon. Not. R. Astron. Soc.* **498**, 4492 (2020).
- [45] J. Skilling, *Bayesian Anal.* **1**, 833 (2006).
- [46] B. P. Abbott *et al.* (LIGO Scientific, Virgo Collaborations), *Classical Quantum Gravity* **37**, 055002 (2020).
- [47] S. Kroker and R. Nawrodt, *IEEE Instrum. Measur. Mag.* **18**, 4 (2015).
- [48] S. Hild, S. Chelkowski, and A. Freise, [arXiv:0810.0604](https://arxiv.org/abs/0810.0604).